Original scientific paper
https://doi.org/10.33180/InfMIDEM2024.401

Informacije MIDEM
Journal of Microelectronics, Electronic Components and Materials
Vol. 54, No. 4(2024), 237 – 245

Electrocaloric and pyroelectric properties of $0.6Ba_{0.85}Ca_{0.15}Zr_{0.10}Ti_{0.90}O_3$ –$0.4BaTi_{0.89}Sn_{0.11}O_3$ ceramics

Soukaina Merselmiz[1,2], Zouhair Hanani[2], Hana Uršič[2,3], Uroš Prah[2], Daoud Mezzane[1,4], El-houssaine Ablouh[5], Matjaž Spreitzer[2], Lahoucine Hajji[1], Zahra Abkhar[1], Brigita Rožič[2], Mimoun El Marssi[4] and Zdravko Kutnjak[2]

[1]IMAD-Lab, Cadi Ayyad University, Marrakesh, Morocco
[2]Jožef Stefan Institute, Ljubljana, Slovenia
[3]Jožef Stefan International Postgraduate School, Ljubljana, Slovenia
[4]LPMC, University of Picardy Jules Verne, Amiens, France
[5]MSN, Mohammed VI Polytechnic University (UM6P), Benguerir, Morocco

Abstract: Ferroelectric materials are gaining considerable attention for energy storage, electrocaloric and pyroelectric energy harvesting applications. In particular, $Ba_{0.85}Ca_{0.15}Zr_{0.10}Ti_{0.90}O_3$ (BCZT) and $BaTi_{0.89}Sn_{0.11}O_3$ (BTSn) ceramics are among the best-studied lead-free $BaTiO_3$-based ferroelectrics with high piezoelectric and electrocaloric properties. In this work, we prepared a 0.6BCZT–0.4BTSn solid solution. The structural, energy storage, electrocaloric, and pyroelectric properties are investigated. An energy density of 61.4 mJ cm^{-3} with a high energy efficiency of 82.4 % at 90 °C is achieved. The electrocaloric temperature change, which is determined indirectly via the Maxwell relation, is 0.5 K at 86 °C and 25 kV cm^{-1}. It is stable over a wide temperature range of around 65 °C and has a coefficient of performance of 15. Moreover, a pyroelectric energy density of 124.1 mJ cm^{-3} is achieved. The results of this study show that the 0.6BCZT–0.4BTSn ceramics is a multifunctional material with energy storage, electrocaloric and pyroelectric properties.

Keywords: Lead-free; ceramic; BCZT; energy storage; electrocaloric; pyroelectric; energy harvesting

Elektrokalorične in piroelektrične lastnosti $0.6Ba_{0.85}Ca_{0.15}Zr_{0.10}Ti_{0.90}O_3$ –$0.4BaTi_{0.89}Sn_{0.11}O_3$ keramike

Izvleček: Feroelektrični materiali pridobivajo veliko pozornost v raziskavah, ki se osredotočajo na elektrokalorične in piroelektrične pojave ter na shranjevanje energije. Zlasti keramiki $Ba_{0.85}Ca_{0.15}Zr_{0.10}Ti_{0.90}O_3$ (BCZT) in $BaTi_{0.89}Sn_{0.11}O_3$ (BTSn) sodita med najbolj raziskane keramične materiale brez svinca na osnovi $BaTiO_3$. V tem delu smo pripravili trdno raztopino 0.6BCZT–0.4BTSn. Raziskali smo strukturne, elektrokalorične in piroelektrične lastnosti keramike 0.6BCZT-0.4BTSn ter njeno zmožnost shranjevanja energije. Keramika izkazuje gostoto shranjevanja energije v višini 61.4 mJ cm^{-3} z najvišjim energijskim izkoristkom 82.4 % pri temperaturi 90 °C. Elektrokalorična temperaturna sprememba določena preko Maxwellove enačbe, znaša 0.5 K pri temperature 86 °C in električnem polju 25 kV cm^{-1} ter je stabilna v širokem temperaturnem območju 65 °C s koeficientom učinkovitosti 15. Keramika izkazuje tudi piroelektrično gostoto energije 124.1 mJ cm^{-3}. Rezultati kažejo, da je keramika 0.6BCZT-0.4BTSn večfunkcijski material, ki izkazuje elektrokalorične in piroelektrične lastnosti ter zmožnost shranjevanja energije.

Ključne besede: keramika brez svinca; BCZT; shranjevanje energije; elektrokalorik; piroelektrik; zbiranje energije

** Corresponding Author's e-mail: soukaina.merselmiz@ijs.si; hana.ursic@ijs.si*

How to cite:
S. Merselmiz et al., "Electrocaloric and pyroelectric properties of $0.6Ba_{0.85}Ca_{0.15}Zr_{0.10}Ti_{0.90}O_3$ –$0.4BaTi_{0.89}Sn_{0.11}O_3$ ceramics", Inf. Midem-J. Microelectron. Electron. Compon. Mater., Vol. 54, No. 4(2024), pp. 237–245

1 Introduction

To alleviate growing environmental concerns, the green energy industry is developing rapidly [1]–[4]. In particular, high-efficiency electrocaloric (EC) cooling technologies have attracted much attention, especially in ferroelectric materials. This is due to their ability to be efficiently driven by electric fields that are readily available, making them promising for use in solid-state cooling systems to cool microelectronic devices [5]–[7]. This is due to their polarization and entropy change near the ferroelectric phase transition upon application/removal of an electric field, resulting in an adiabatic temperature change (ΔT), known as the EC effect [8]–[10]. In addition, dielectric capacitors such as ferroelectric materials have been widely used in energy-scavenging technologies based solely on their intrinsic polarization [11], [12].

The waste heat produced by many electronic devices presents an opportunity for energy harvesting technologies, which can convert it in various ways [13]. One approach to enhance device efficiency, involves harvesting and converting this wasted heat through pyroelectric energy harvesting [14], [15]. This method requires converting heat energy into clean electricity using materials exhibiting the pyroelectric effect [16]. This effect known as the converse of the EC effect, involves the transformation of waste or heat energy into electrical voltage when subjected to temperature variations [17]. Its magnitude can be assessed using the Olsen cycle, similar to the Ericson cycle [18], [19]. Accordingly, the density of pyroelectric energy harvesting (U_{pyro}) can be calculated from the recorded polarization–electric field (P–E) hysteresis loop of ferroelectric materials. Since ferroelectrics are a subgroup of pyroelectrics, $BaTiO_3$ (BT)-based materials are considered promising candidates for pyroelectric energy harvesting. These materials exhibit significant spontaneous polarization and can undergo polarization changes across a broad temperature range, fulfilling the requirements of the EC effect. For example, U_{pyro} value of 229 mJ cm^{-3} was found in $0.5BaZr_{0.2}Ti_{0.8}O_3$–$0.5Ba_{0.7}Ca_{0.3}TiO_3$ ceramics [20]. In addition, a comparable U_{pyro} value of 210 mJ cm^{-3} was obtained in $BaTi_{0.91}Sn_{0.09}O_3$ ceramics [21].

Ceramic dielectric capacitors play crucial roles as energy conversion and storage devices by absorbing and releasing large voltages or current pulses within a short lifetime between microseconds and milliseconds [22]. This property makes them promising candidates for energy-storage devices within pulsed-power and power-conditioning electronic applications [2], [23]. Pure BT ceramics capacitors exhibit a ferroelectric tetragonal phase with high dielectric permittivity close to the Curie temperature (T_c) and a relatively square-like P–E hysteresis loop, with both large remanent polarization (P_r) and coercive field (E_c). These properties lead to high energy loss (U_{loss}), low recovered energy density (U_{rec}) as well as low energy storage efficiency (η), limiting BT ceramics from practical application in energy storage devices [24]. Doping BT material with Ca^{2+} at the A-site and with Zr^{4+}/Sn^{4+} at the B-site could be beneficial to adjust the P–E hysteresis loop by reducing the P_r and increasing the difference ΔP between the maximal polarization (P_{max}) and P_r, thereby enhancing simultaneously its U_{rec} and η [22], [24]–[27].

In 2009, Liu et al. reported a high piezoelectric coefficient of d_{33} ~ 620 pC N^{-1} in $Ba_{0.85}Ca_{0.15}Zr_{0.10}Ti_{0.90}O_3$ (abbreviated as BCZT) ceramics related to the morphotropic phase boundary occurring at room temperature. Subsequently, $BaTi_{0.89}Sn_{0.11}O_3$ (abbreviated as BTSn) with a quasi-quadruple point (coexistence of cubic–tetragonal–orthorhombic–rhombohedral phases) was found to have high dielectric permittivity (~ 75 000) and improved piezoelectric coefficient of d_{33} ~ 697 pC N^{-1} at ~ 42 °C [28]. As a result, the chemical modification of BT (e.g., Ca, Zr, Sn, etc.) enhance further the dielectric and piezoelectric poperties [29]–[35]. With the chemical modification, the thermal stability of the properties can be tailored by approaching the rhombohedral–orthorhombic (R–O, T_{R-O}) and orthorhombic–tetragonal (O–T, T_{O-T}) phase boundaries with the corresponding phase transition temperatures to the T_c peak temperature together with shifting T_c to room temperature [31]. The sequence of phase boundaries enhance the thermal stability of the properties over a wide temperature range, which is essential to achieve practical applications [31].

We have previously reported the EC properties of BCZT and BTSn ceramics studied by the indirect Maxwell approach [36], [37]. BTSn ceramics showed high ΔT~0.71 K at 40 °C at 25 kV cm^{-1}, but in a relatively narrow temperature span (T_{span}) [37]. Meanwhile, BTSn ceramic showed a U_{rec} of 84.4 mJ cm^{-3} with high η of 91.0 %. In contrast, BCZT ceramics showed a ΔT~0.57 K at 100 °C at the same electric field in a relatively broader T_{span} of 70 K [36]. However, the U_{rec} was ~75 mJ cm^{-3} with a very low η of 37 %, limiting BCZT from practical applications. In order to prepare multifunctional material with both enhanced electrical properties and thermal stability, we prepared $(1-x)Ba_{0.85}Ca_{0.15}Zr_{0.10}Ti_{0.90}O_3$–$xBaTi_{0.89}Sn_{0.11}O_3$ solid solution system (x = 0.2, 0.4 and 0.6) as previously reported in our previous work [38]. In this work, we investigated structural, energy storage, EC effect and pyroelectric energy harvesting properties of 0.6BCZT-0.4BTSn ceramics (abbreviated as 0.4BTSn).

2 Materials and methods

The $0.6Ba_{0.85}Ca_{0.15}Zr_{0.10}Ti_{0.90}O_3$–$0.4BaTi_{0.89}Sn_{0.11}O_3$ (abbreviated as 0.4BTSn) ceramics was prepared by conventional solid-state method, by homogenizing BCZT and BTSn calcined powders. The preparation process of 0.4BTSn ceramics is described in detail in our previous work [38].

The crystalline structure of crushed 0.4BTSn ceramic pellet at room-temperature (RT) was investigated by X-ray powder diffractometer (XRD, BRUKER AXS D4 ENDEAVOR) equipped with Cu-Kα-radiation. Diffraction patterns were recorded in the 10–80° *2θ*-range with a step size of 0.02° using Cu-Kα-radiation. Phase identification was performed with the COD-2020 database using the standard diffraction peaks of $BaTiO_3$ with orthorhombic (PDF#81–2200) and tetragonal (PDF#05–0626) symmetries [39].

The microstructure of sintered ceramics was examined using a scanning electron microscope (SEM, Zeiss EVO 10 SEM, Carl Zeiss Microscopy, Germany) equipped with an energy dispersive X-ray spectrometer (EDXS, ZEISS SmartEDX Instrument, Carl Zeiss Microscopy, Germany). Prior to the microstructural analysis, the samples were ground and finely polished using a colloidal silica suspension. The bulk density of the sintered ceramics was determined by the Archimedes' method using deionized water as medium. In addition, the average grain size was determined from the digitized images of the polished surfaces processed with ImageJ software (version 1.52a, National Institutes of Health, USA) by measuring more than 300 grains using the average grain intercept (AGI) method.

For the electrical properties, the ceramic pellets were cut, thinned, and polished to a thickness of about 400 µm and then the Cr/Au electrodes were sputtered on sample' surfaces. The dielectric properties were measured using a precision LCR Meter instrument (Agilent, 4284A, USA) in the temperature range from –50 to 200 °C. The polarization versus electric field (*P*–*E*) hysteresis loops were recorded using Aixacct TF analyzer 2000 (Aixacct, Aachen, Germany) from 30 to 140 °C using a triangular excitation signal with a frequency of 10 Hz.

3 Results

The XRD patterns of the 0.4BTSn ceramic at room temperature is shown in Figure 1 (a). It shows peaks characteristic of the perovskite phase. The XRD fitting pattern extended by $2\theta \approx 45°$ using the Lorentz fitting method is shown in the inset (Figure 1 (b)). The enlarged peak presents a splitting of two peaks that could be the coexistence of orthorhombic $(022)_O$ and tetragonal $(200)_T$ peaks

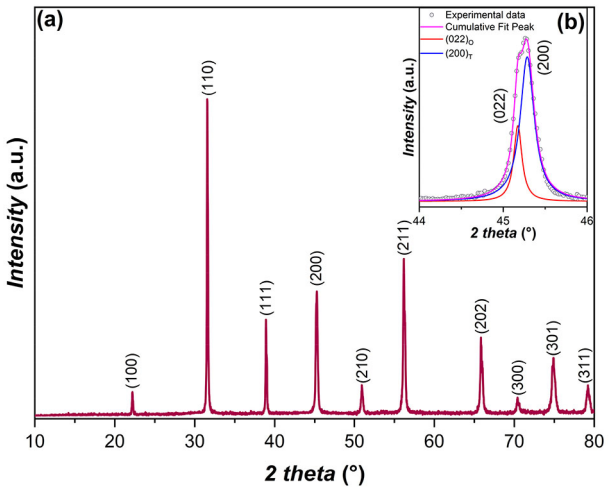

Figure 1: (a) Room-temperature XRD pattern of the 0.4BTSn ceramics, and (b) the enlarged view of the peak splitting at $2\theta \approx 45°$.

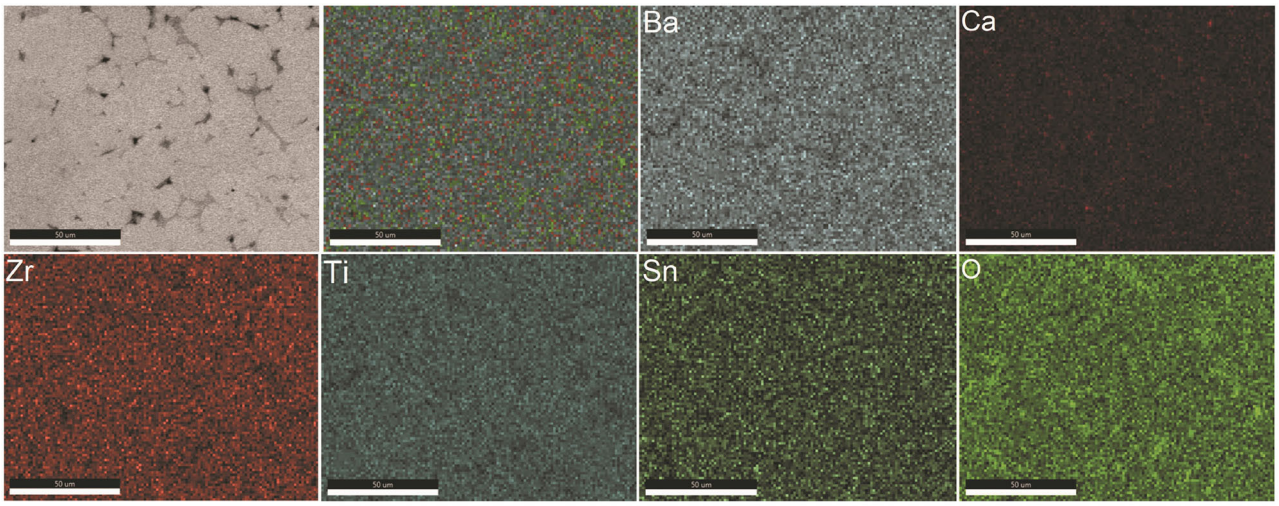

Figure 2: SEM image and EDXS maps show the distribution of elements Ba, Ca, Zr, Ti, Sn and O on the surface of the 0.4BTSn ceramic (Scale bar: 50 µm).

forming a $(022)_O/(200)_T$ doublet [40]. These results were confirmed by using Rietveld refinement, as reported in our previous work [38].

To gain insight into the microstructure and chemical composition of the 0.4BTSn ceramics, Figure 2 shows the SEM and the elemental mapping images on the polished surface of the sample. A compact and dense microstructure with an average grain size of (12.0 ± 4.8) μm were observed. The density of the ceramic was 5.5 g cm^{-3}, which corresponds to 93 % of the theoretical density. Furthermore, the EDXS mapping images show a homogeneous distribution of all contained elements (Ba, Ca, Zr, Ti, Sn and O).

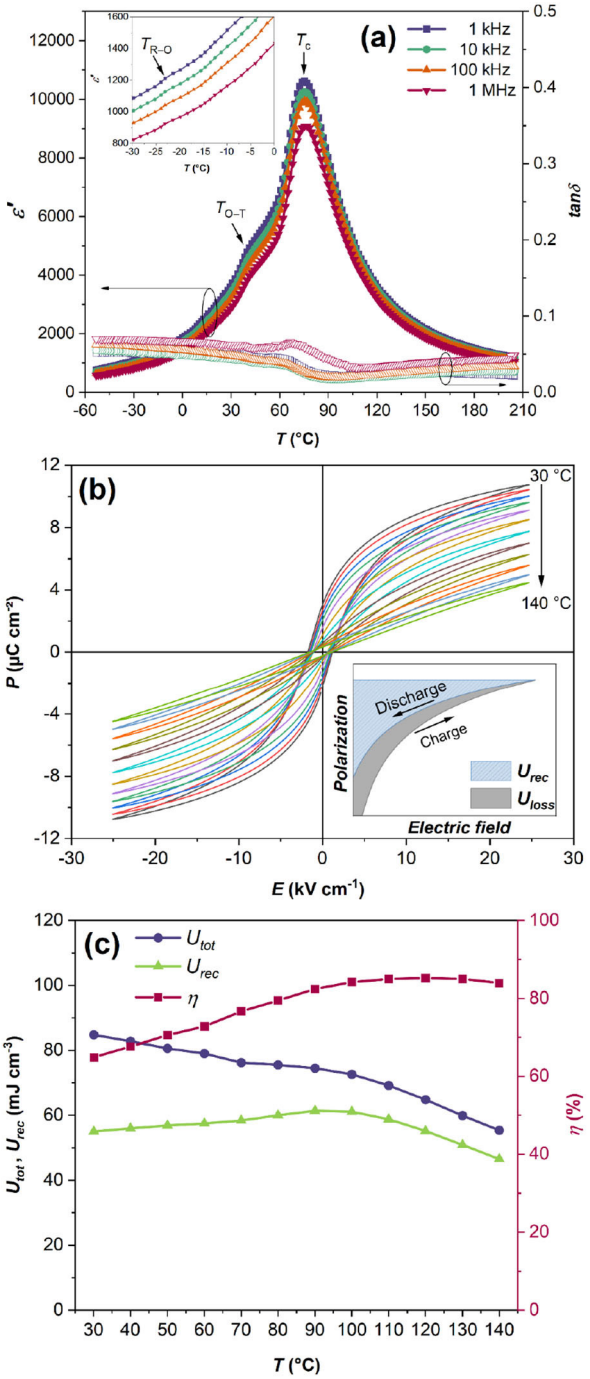

Figure 3: Temperature dependence of (a) *ε´* and *tanδ*, and (b) *P–E* hysteresis loops for 0.4BTSn ceramics. Inset: A schematic depiction of the relevant U_{rec} and U_{loss} determined via *P–E* hysteresis loops. (c) The corresponding energy storage properties as a function of temperature.

The temperature dependence of the dielectric permittivity (*ε´*) and dielectric loss (*tanδ*) of the 0.4BTSn sample are shown in Figure 3 (a). Sequential anomalies corresponding to R–O (T_{R-O}), O–T (T_{O-T}), and tetragonal-cubic (T_c) phase transitions at about –23, 37, and 75 °C, respectively, are observed. The maximum value of permittivity (ε'_{max}) and the peak-permittivity temperature (T_m) were found to be ~ 10630 at ~ 77 °C and 1 kHz, corresponding to a dielectric loss of *tanδ* ~ 0.04.

P–E hysteresis loops at different temperatures are shown in Figure 3 (b). As the temperature increases, the P_{max} decreases continuously due to the ferroelectric-paraelectric phase transition above temperatures around ~ 80 °C. To further investigate the energy storage properties, the recorded *P–E* hysteresis loops as a function of applied electric field and temperature were used. Inset in Figure 3 (b) shows schematically the areas presenting the U_{rec} and the U_{loss} in blue and gray colors, respectively. The total energy density (U_{tot}) can be calculated by integrating and gathering U_{rec} and U_{loss} areas using equations (1) and (2). Therefore, the η can be estimated using equation (3) [41]. The temperature dependence of the energy storage properties is plotted in Figure 3 (c). At room temperature, the U_{rec} value was found to be ~ 55 mJ cm^{-3} with η ~ 65 %, which is twice as high as that of pure BCZT (η ~ 37 %) at 25 kV cm^{-1} [36]. At 120 °C, high η value of 86 % was found in 0.4BTSn ceramic, exceeding that of pure BCZT (η ~ 72%) [36].

$$U_{tot} = \int_0^{P_{max}} EdP \quad (1)$$

$$U_{rec} = \int_{P_r}^{P_{max}} EdP \quad (2)$$

$$\eta\,(\%) = \frac{U_{rec}}{U_{tot}} \times 100 = \frac{U_{rec}}{U_{rec} + U_{loss}} \times 100 \quad (3)$$

For environmentally friendly solid-state cooling devices, the electrocaloric properties of 0.4BTSn ceramics were indirectly evaluated via the Maxwell relation using the measured electric polarization *P* (*T*, *E*). First, a fifth-order polynomial fit of the upper polarization branches was performed at each fixed applied electric field [5]. The thermal evolution of the polarization was

derived. The polarization (*P*) decreases continuously with increasing temperature as presented in Figure 4 (a). The isothermal entropy change (*ΔS*) and the *ΔT* were estimated using Maxwell relation with equations (4) and (5), where *E*, *ρ* and C_p denote the applied electric field, mass density and specific heat of the sample, respectively [5]. The value of C_p (0.48 J g^{-1} K^{-1}) was taken from Ref. [42].

$$\Delta S = \int_{E_1}^{E_2} \left(\frac{\partial P}{\partial T} \right)_E dE \tag{4}$$

$$\Delta T = -\int_{E_1}^{E_2} \frac{T}{\rho C_p} \left(\frac{\partial P}{\partial T} \right)_E dE \tag{5}$$

Figure 4 (b) shows the temperature dependence of *ΔT* at different applied electric fields. The T_{O-T} and T_c are visible and more pronounced with increasing the applied *E*. The maximum *ΔT* was found to be around the T_c. As the *E* increases, *ΔT* increases and its maxima

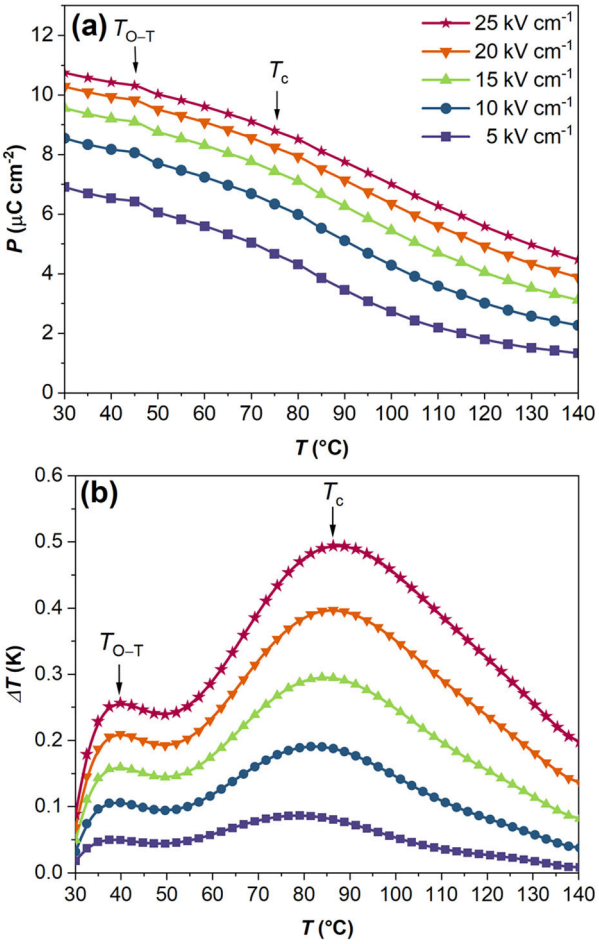

Figure 4: Temperature dependence of (a) *P* and (b) *ΔT* of the 0.4 BTSn ceramics measured at different applied electric fields from 5 to 25 kV cm^{-1}, showing the transition temperatures T_{O-T} and T_c.

shift slightly to higher temperatures. At 25 kV cm^{-1}, *ΔT* reaches a maximum of 0.5 K at 86 °C, then gradually decreases. A crucial parameter for evaluating the EC effect of a material is the EC responsivity, written as $\zeta = \Delta T/\Delta E$. This calculated coefficient was found to be $\zeta = 0.20$ K mm kV^{-1} at the peak temperature. Table 1 presents comparable results for some of the previously published EC outcomes for lead-free ferroelectric materials compared to 0.4BTSn ceramics.

For practical cooling applications, maintaining a significant EC effect over a wide temperature range (T_{span}) is of great importance. T_{span} is usually specified as the full width at half maximum (FWHM) of the EC peak (at the FE–PE phase transition), which can exceed 45–60 °C at a high EC effect benchmark [43]. The diffuse phase transition has been found to be directly related to the broadened EC peaks at low electric fields [44]. Improved T_{span} value of 65 °C is obtained, which could be explained by the successive phase transitions and to the diffuse phase transition.

Another important parameter for evaluating the suitability of EC materials for use in solid-state refrigeration systems, is the refrigerant capacity $RC = \Delta S.\ T_{span}$ [5]. This parameter *was* found to be 33.1 J kg^{-1}. In addition, the coefficient of performance (*COP* = input power/output cooling power = $|T.\Delta S|/|U_{rec}|$) is considered a crucial parameter for estimating the refrigeration cycle performance and evaluating the efficiency of the material [5]. The calculated *COP* value is 15 at 90 °C, which is higher than some other lead-free [45]–[47]. In summary, the 0.4BTSn ceramics could be an advantageous material for some specific EC cooling systems in a wide temperature range.

Ferroelectric materials with enhanced polarization change upon heating have a high potential for use in pyroelectric energy harvesting [18]. For this reason, the pyroelectric energy harvesting performances of 0.4BTSn ceramic were evaluated. The magnitude of the pyroelectric effect can be evaluated using the Olsen cycle. Figure 5 (a) depicts a diagram illustrating the functioning of the pyroelectric energy harvesting effect employing the Olsen cycle. It involves two isothermal (A→B, C→D) and two isoelectric (B→C, D→A) processes per cycle [18]. The pyroelectric energy density (U_{pyro}), which is achieved in certain temperature and electric field ranges, corresponds to the area A→B→C→D→A, which can be described by equation (6) [48]. The U_{pyro} divided by the total heat energy that is absorbed by this process gives the pyroelectric energy efficiency (η_{pyro}) (see equation 7). Analogous to the EC effect, we define the pyroelectric responsivity (ζ_{pyro}) by the equation (8), when the energy harvesting density can be rationalized by the temperature change of the corresponding Olsen cycle,

$$U_{pyro} = \oint EdP \quad (6)$$

$$\eta_{pyro} = \frac{U_{pyro}}{\rho C_p \left(T_H - T_L\right)} \quad (7)$$

$$\zeta_{pyro} = \frac{U_{pyro}}{\Delta E.\Delta T} \quad (8)$$

Figure 5 (b) shows the high-temperature dependence of U_{pyro} and η_{pyro} at T_L = 30 °C, E_L = 5 kV cm^{-1} and E_H = 25 kV cm^{-1} in 0.4BTSn ceramic. It is observed that U_{pyro} increases with T_H, and the maximum U_{pyro} value is 124.1 mJ cm^{-3} at T_H = 140 °C. Meanwhile, η_{pyro} increases andreaches a maximum value of 0.08 % at T_H = 120 °C. Accordingly, ζ_{pyro} is calculated to be 0.56 × 10^{-7} J cm^{-2} V^{-1} K^{-1}. The obtained pyroelectric energy harvesting parameters are improved compared to some reported lead-free $BaTiO_3$-based ceramics [48], [53], [54]. Accordingly, 0.4BTSn ceramic has the potentials to be used as a working material in pyroelectric energy harvesting applications.

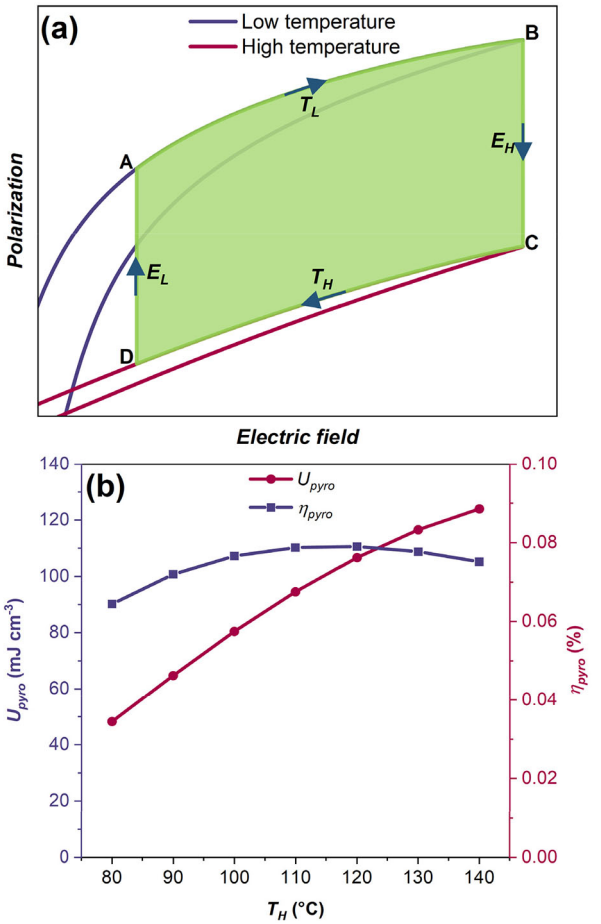

Figure 5: (a) A diagram illustrating the principle of pyroelectric energy harvesting using *P–E* hysteresis loops measured at two different temperatures based on the Olsen cycle. The green region represents the U_{pyro}. (b) The high-temperature dependence of U_{pyro} and η_{pyro} of 0.4BTSn ceramics between 5 and 25 kV cm^{-1}.

4 Conclusions

In summary, the multifunctional lead-free 0.4BTSn ceramic was prepared by the solid-state reaction method. The energy storage, electrocaloric and pyroelectric energy harvesting properties were systematically investigated. Increased energy storage performances (U_{rec} = 61.4 mJ cm^{-3} and η = 82.4 % at 90 °C), electrocaloric properties (ΔT = 0.50 K, ζ = 0.20 K mm kV^{-1}, RC = 33.1 J kg^{-1} and COP = 15 at T_c = 86 °C with T_{span} = 64.9 °C) as well as pyroelectric energy harvesting performances (U_{pyro} = 124.1 mJ cm^{-3}, η_{pyro} = 0.08 % and ζ_{pyro} = 0.56 × 10^{-7} J cm^{-2} V^{-1} K^{-1} at T_L = 30 °C and T_H = 140 °C) were obtained. These results indicate that the 0.4BTSn sample is a good, eco-friendly, and thermally-stable multifunctional ferroelectric material for energy storage, electrocaloric, and pyroelectric applications.

Table 1: Comparison of the electrocaloric properties of 0.4BTSn ceramics with other lead-free BT-based ceramics reported in the literature.

Ceramic	T_c (°C)	ΔT (K)	ΔE (kV cm^{-1})	ζ (K mm V^{-1})	Ref.
$Ba_{0.94}Ca_{0.06}Ti_{0.90}Sn_{0.10}O_3$	47	0.55	20	0.280	[49]
$Ba_{0.85}Ca_{0.15}Zr_{0.10}Ti_{0.90}O_3-0.4BaTi_{0.89}Sn_{0.11}O_3$	86	0.50	25	0.200	This work
$BaTi_{0.89}Sn_{0.11}O_3$	52	0.71	25	0.284	[37]
$Ba_{0.85}Ca_{0.15}Zr_{0.10}Ti_{0.90}O_3$	100	0.57	25	0.228	[36]
0.8$Ba(Ti_{0.89}Sn_{0.11})O_3$–0.2$(Ba_{0.7}Ca_{0.3})TiO_3$	65	0.63	25	0.025	[43]
0.3$BaHf_{0.2}Ti_{0.8}O_3$–0.7$Ba_{0.94}Sm_{0.04}TiO_3$	64	0.46	30	0.180	[47]
$Ba_{0.97}Ce_{0.03}Ti_{0.99}Mn_{0.01}O_3$	55	0.41	30	0.140	[50]
$Ba_{0.85}Ca_{0.15}Zr_{0.1}Ti_{0.88}Sn_{0.02}O_3$	80	0.84	32	0.262	[44]
$Ba_{0.7}Sr_{0.3}TiO_3$	40	0.67	40	0.160	[51]
$Ba_{0.82}Ca_{0.18}Sn_{0.065}Ti_{0.935}O_3$	30	0.59	50	0.118	[52]

5 Acknowledgments

The authors would like to thank the CNRST Priority Program PPR 15/2015, the Slovenian research agency grants (No. P2-0105, No. N2-0212 and No. P1-0125, No. J1-9147, No. P2-0091) and the European Union Horizon 2020 Research and Innovation actions MSCA-RISE-ENGIMA (No. 778072) and MSCA-RISE-MELON (No. 872631).

6 Conflict of interest

The authors declare no conflict of interest.

7 References

1. B. Malič, M. Otoničar, K. Radan, and J. Koruza, "Lead-Free Piezoelectric Ceramics," in *Encyclopedia of Materials: Technical Ceramics and Glasses*, (Ed.: M. Pomeroy), Ed. Amsterdam: Elsevier BV, 2021, pp. V3-358-V3-368, https://doi.org/10.1016/B978-0-12-803581-8.12131-9.
2. S. Zhang, B. Malič, J. F. Li, and J. Rödel, "Lead-free ferroelectric materials: Prospective applications," *J. Mater. Res.*, vol. 36, no. 5, pp. 985–995, Mar. 2021, https://doi.org/10.1557/s43578-021-00180-y.
3. J. Rödel, W. Jo, K. T. P. Seifert, E. M. Anton, T. Granzow, and D. Damjanovic, "Perspective on the development of lead-free piezoceramics," *J. Am. Ceram. Soc.*, vol. 92, no. 6, pp. 1153–1177, Jun. 2009, https://doi.org/10.1111/j.1551-2916.2009.03061.x.
4. J. Rödel and J. F. Li, "Lead-free piezoceramics: Status and perspectives," *MRS Bull.*, vol. 43, no. 8, pp. 576–580, Aug. 2018, https://doi.org/10.1557/mrs.2018.181.
5. Z. Kutnjak, B. Rožič, and R. Pirc, "Electrocaloric Effect: Theory, Measurements, and Applications," in *Wiley Encyclopedia of Electrical and Electronics Engineering*, Hoboken, NJ, USA: John Wiley & Sons, Inc., 2015, pp. 1–19, https://doi.org/10.1002/047134608x.w8244.
6. X. Moya and N. D. Mathur, "Caloric materials for cooling and heating," *Science (80-.).*, vol. 370, no. 6518, pp. 797–803, Nov. 2020, https://doi.org/10.1126/science.abb0973.
7. A. Torelló and E. Defay, "Electrocaloric Coolers: A Review," *Adv. Electron. Mater.*, vol. 8, no. 6, Jun. 2022, https://doi.org/10.1002/aelm.202101031.
8. Z. Kutnjak and B. Rožič, "Indirect and Direct Measurements of the Electrocaloric Effect," in *Engineering Materials*, (Ed.:Tatiana Correia and Qi Zhang), Ed. Berlin, Heidelberg: Springer, 2014, pp. 147–182, https://doi.org/10.1007/978-3-642-40264-7_7.
9. A. L. Kholkin, O. V. Pakhomov, A. A. Semenov, and A. Tselev, "The Electrocaloric Effect: Materials and Applications," *Electrocaloric Eff. Mater. Appl.*, pp. 1–433, 2023, https://doi.org/10.1016/C2019-0-02843-9.
10. X. Chen, V. V. Shvartsman, D. C. Lupascu, and Q. M. Zhang, "Electrocaloric cooling - From materials to devices," *J. Appl. Phys.*, vol. 132, no. 24, Dec. 2022, https://doi.org/10.1063/5.0132533.
11. Z. Fan, X. Liu, and X. Tan, "Large electrocaloric responses in [Bi1/2(Na,K)1/2]TiO3-based ceramics with giant electro-strains," *J. Am. Ceram. Soc.*, vol. 100, no. 5, pp. 2088–2097, May 2017, https://doi.org/10.1111/jace.14777.
12. M. S. Habib *et al.*, "Experimental determination of electrophoretic deposition parameters and electrical characterization for K 0.5 Na 0.5 NbO3 perovskite thick films for energy harvesting applications," *Mater. Chem. Phys.*, vol. 316, p. 129074, Apr. 2024, https://doi.org/10.1016/j.matchemphys.2024.129074.
13. S. Pandya *et al.*, "New approach to waste-heat energy harvesting: pyroelectric energy conversion," *NPG Asia Mater.*, vol. 11, no. 1, p. 26, Dec. 2019, https://doi.org/10.1038/s41427-019-0125-y.
14. F. Y. Lee, A. Navid, and L. Pilon, "Pyroelectric waste heat energy harvesting using heat conduction," *Appl. Therm. Eng.*, vol. 37, pp. 30–37, May 2012, https://doi.org/10.1016/j.applthermaleng.2011.12.034.
15. P. Lheritier *et al.*, "Large harvested energy with non-linear pyroelectric modules," *Nature*, vol. 609, no. 7928, pp. 718–721, Sep. 2022, https://doi.org/10.1038/s41586-022-05069-2.
16. D. Zhang, H. Wu, C. R. Bowen, and Y. Yang, "Recent Advances in Pyroelectric Materials and Applications," *Small*, vol. 17, no. 51, Dec. 2021, https://doi.org/10.1002/smll.202103960.
17. S. P. Alpay, J. Mantese, S. Trolier-McKinstry, Q. Zhang, and R. W. Whatmore, "Next-generation electrocaloric and pyroelectric materials for solid-state electrothermal energy interconversion," *MRS Bull.*, vol. 39, no. 12, pp. 1099–1111, Dec. 2014, https://doi.org/10.1557/mrs.2014.256.
18. C. R. Bowen, J. Taylor, E. Leboulbar, D. Zabek, A. Chauhan, and R. Vaish, "Pyroelectric materials and devices for energy harvesting applications," *Energy Environ. Sci.*, vol. 7, no. 12, pp. 3836–3856, 2014, https://doi.org/10.1039/c4ee01759e.
19. S. Patel *et al.*, "Thermomechanical Energy Conversion Potential of Lead-Free 0.50Ba(Zr0.2Ti0.8) O3–0.50(Ba0.7Ca0.3)TiO3 Bulk Ceramics," *Energy Technol.*, vol. 6, no. 5, pp. 872–882, May 2018, https://doi.org/10.1002/ente.201700416.

20. D. Ando and K. ichi Kakimoto, "Pyroelectric energy harvesting using low–TC (1–x)(Ba0.7Ca0.3)TiO3–xBa(Zr0.2Ti0.8)O3 bulk ceramics," *J. Am. Ceram. Soc.*, vol. 101, no. 11, pp. 5061–5070, Nov. 2018, https://doi.org/10.1111/jace.15746.
21. H. Kacem *et al.*, "Relaxor characteristics and pyroelectric energy harvesting performance of $BaTi_{0.91}Sn_{0.09}O_3$ ceramic," *J. Alloys Compd.*, vol. 872, p. 159699, 2021, https://doi.org/10.1016/j.jallcom.2021.159699.
22. F. Yan, J. Qian, S. Wang, and J. Zhai, "Progress and outlook on lead-free ceramics for energy storage applications," *Nano Energy*, vol. 123, p. 109394, May 2024, https://doi.org/10.1016/j.nanoen.2024.109394.
23. L. Yang *et al.*, "Perovskite lead-free dielectrics for energy storage applications," *Prog. Mater. Sci.*, vol. 102, pp. 72–108, May 2019, https://doi.org/10.1016/j.pmatsci.2018.12.005.
24. H. Zhang *et al.*, "A review on the development of lead-free ferroelectric energy-storage ceramics and multilayer capacitors," *J. Mater. Chem. C*, vol. 8, no. 47, pp. 16648–16667, 2020, https://doi.org/10.1039/d0tc04381h.
25. A. Jain, Y. G. Wang, and L. N. Shi, "Recent developments in BaTiO3 based lead-free materials for energy storage applications," *J. Alloys Compd.*, vol. 928, 2022, https://doi.org/10.1016/j.jallcom.2022.167066.
26. V. Veerapandiyan, F. Benes, T. Gindel, and M. Deluca, "Strategies to improve the energy storage properties of perovskite lead-free relaxor ferroelectrics: A review," *Materials (Basel).*, vol. 13, no. 24, pp. 1–47, Dec. 2020, https://doi.org/10.3390/ma13245742.
27. V. Veerapandiyan *et al.*, "Origin of Relaxor Behavior in Barium-Titanate-Based Lead-Free Perovskites," *Adv. Electron. Mater.*, vol. 8, no. 2, Feb. 2022, https://doi.org/10.1002/aelm.202100812.
28. Y. Yao *et al.*, "Large piezoelectricity and dielectric permittivity in BaTiO 3-xBaSnO 3 system: The role of phase coexisting," *Epl*, vol. 98, no. 2, 2012, https://doi.org/10.1209/0295-5075/98/27008.
29. T. R. Shrout and S. J. Zhang, "Lead-free piezoelectric ceramics: Alternatives for PZT?," *J. Electroceramics*, vol. 19, no. 1, pp. 111–124, Sep. 2007, https://doi.org/10.1007/s10832-007-9047-0.
30. Y. Zhang, L. Chen, H. Liu, S. Deng, H. Qi, and J. Chen, "High-performance ferroelectric based materials via high-entropy strategy: Design, properties, and mechanism," *InfoMat*, vol. 5, no. 12, Dec. 2023, https://doi.org/10.1002/inf2.12488.
31. C. Zhao, B. Wu, and J. Wu, "Composition-driven broad phase boundary for optimizing properties and stability in lead-free barium titanate ceramics," *J. Am. Ceram. Soc.*, vol. 102, no. 6, pp. 3477–3487, 2019, https://doi.org/10.1111/jace.16194.
32. M. Acosta *et al.*, "BaTiO3-based piezoelectrics: Fundamentals, current status, and perspectives," *Appl. Phys. Rev.*, vol. 4, no. 4, Dec. 2017, https://doi.org/10.1063/1.4990046.
33. G. Canu *et al.*, "Structure-property correlations and origin of relaxor behaviour in BaCexTi1-xO3," *Acta Mater.*, vol. 152, pp. 258–268, Jun. 2018, https://doi.org/10.1016/j.actamat.2018.04.038.
34. S. W. Konsago, A. Debevec, J. Cilenšek, B. Kmet, and B. Malič, "Linear Thermal Expansion of 0.5Ba(Zr0.2Ti0.8)O3-0.5(Ba0.7Ca0.3)TiO3 Bulk Ceramic," *Inf. MIDEM*, vol. 53, no. 4, pp. 233–238, Feb. 2023, https://doi.org/10.33180/InfMIDEM2023.403.
35. M. S. Habib *et al.*, "Improved sintering and impedance studies of CuO-doped multiferroic (0.98Ba0.85Ca0.15) (Zr0.1Ti0.9)·O30.02BiFeO3 ceramics," *Appl. Phys. A Mater. Sci. Process.*, vol. 128, no. 3, p. 238, Mar. 2022, https://doi.org/10.1007/s00339-022-05370-x.
36. S. Merselmiz *et al.*, "Thermal-stability of the enhanced piezoelectric, energy storage and electrocaloric properties of a lead-free BCZT ceramic," *RSC Adv.*, vol. 11, no. 16, pp. 9459–9468, 2021, https://doi.org/10.1039/D0RA09707A.
37. S. Merselmiz *et al.*, "High energy storage efficiency and large electrocaloric effect in lead-free BaTi0.89Sn0.11O3 ceramic," *Ceram. Int.*, vol. 46, no. 15, pp. 23867–23876, Jun. 2020, https://doi.org/10.1016/j.ceramint.2020.06.163.
38. S. Merselmiz *et al.*, "Design of lead-free BCZT-based ceramics with enhanced piezoelectric energy harvesting performances," *Phys. Chem. Chem. Phys.*, 2022, https://doi.org/10.1039/D1CP04723J.
39. L. F. Zhu, B. P. Zhang, L. Zhao, and J. F. Li, "High piezoelectricity of BaTiO3-CaTiO3-BaSnO 3 lead-free ceramics," *J. Mater. Chem. C*, vol. 2, no. 24, pp. 4764–4771, 2014, https://doi.org/10.1039/c4tc00155a.
40. W. Cai *et al.*, "Effects of oxygen partial pressure on the electrical properties and phase transitions in (Ba,Ca)(Ti,Zr)O3 ceramics," *J. Mater. Sci.*, vol. 55, no. 23, pp. 9972–9992, Aug. 2020, https://doi.org/10.1007/s10853-020-04771-8.
41. H. Palneedi, M. Peddigari, G. T. Hwang, D. Y. Jeong, and J. Ryu, "High-Performance Dielectric Ceramic Films for Energy Storage Capacitors: Progress and Outlook," *Adv. Funct. Mater.*, vol. 28, no. 42, p. 1803665, Oct. 2018, https://doi.org/10.1002/adfm.201803665.

42. Y. Zhou, Q. Lin, W. Liu, and D. Wang, "Compositional dependence of electrocaloric effect in lead-free (1 - X)Ba(Zr0.2Ti0.8)O3-x(Ba0.7Ca0.3)TiO3 ceramics," *RSC Adv.*, vol. 6, no. 17, pp. 14084–14089, 2016, https://doi.org/10.1039/c5ra26692k.
43. C. Zhao, J. Yang, Y. Huang, X. Hao, and J. Wu, "Broad-temperature-span and large electrocaloric effect in lead-free ceramics utilizing successive and metastable phase transitions," *J. Mater. Chem. A*, vol. 7, no. 44, pp. 25526–25536, 2019, https://doi.org/10.1039/c9ta10164k.
44. S. Patel, P. Sharma, and R. Vaish, "Enhanced electrocaloric effect in Ba 0.85 Ca 0.15 Zr 0.1 Ti 0.9–x Sn x O 3 ferroelectric ceramics," *Phase Transitions*, vol. 89, no. 11, 2016, https://doi.org/10.1080/01411594.2016.1144752.
45. S. Merselmiz *et al.*, "Enhanced electrical properties and large electrocaloric effect in lead-free Ba0.8Ca0.2ZrxTi1−xO3 (x = 0 and 0.02) ceramics," *J. Mater. Sci. Mater. Electron.*, vol. 31, no. 19, pp. 17018–17028, Oct. 2020, https://doi.org/10.1007/s10854-020-04259-w.
46. L. B. Kong, H. Huang, and S. Li, "Fundamentals of Ferroelectric Materials," in *Ferroelectric Materials for Energy Applications*, Weinheim, Germany: Wiley-VCH Verlag GmbH & Co. KGaA, 2018, pp. 1–31, https://doi.org/10.1002/9783527807505.ch1.
47. B. Zhang *et al.*, "Enhanced electrocaloric effect in the Sm and Hf co-doped BaTiO3 ceramics," *Ceram. Int.*, vol. 47, no. 1, pp. 1101–1108, Jan. 2021, https://doi.org/10.1016/j.ceramint.2020.08.226.
48. P. Wu *et al.*, "Direct and indirect measurement of electrocaloric effect in lead-free (100-x) Ba(Hf0.2Ti0.8)O3-x(Ba0.7Ca0.3)TiO3 ceramics near multi-phase boundary," *J. Alloys Compd.*, vol. 725, pp. 275–282, Nov. 2017, https://doi.org/10.1016/j.jallcom.2017.07.103.
49. X. Wang *et al.*, "Giant electrocaloric effect in lead-free Ba 0.94 Ca 0.06 Ti 1− x Sn x O 3 ceramics with tunable Curie temperature," *Appl. Phys. Lett.*, vol. 107, no. 25, p. 252905, Dec. 2015, https://doi.org/10.1063/1.4938134.
50. S. Liu *et al.*, "Tunable electrocaloric and energy storage behavior in the Ce, Mn hybrid doped BaTiO3 ceramics," *J. Eur. Ceram. Soc.*, vol. 38, no. 14, pp. 4664–4669, Nov. 2018, https://doi.org/10.1016/j.jeurceramsoc.2018.06.020.
51. X. Q. Liu, T. T. Chen, M. Sen Fu, Y. J. Wu, and X. M. Chen, "Electrocaloric effects in spark plasma sintered Ba0.7Sr 0.3TiO3-based ceramics: Effects of domain sizes and phase constitution," *Ceram. Int.*, vol. 40, no. 7 PART B, pp. 11269–11276, Aug. 2014, https://doi.org/10.1016/j.ceramint.2014.03.175.
52. Z. Li, C. Molin, A. Michaelis, and S. E. Gebhardt, "Modified (Ba,Sr)(Sn,Ti)O3 via hydrothermal synthesis for electrocaloric application," *Open Ceram.*, vol. 16, p. 100502, Dec. 2023, https://doi.org/10.1016/j.oceram.2023.100502.
53. Z. Liu *et al.*, " Large electrocaloric and pyroelectric energy harvesting effect over a broad temperature range via modulating the relaxor behavior in non-relaxor ferroelectrics ," *J. Mater. Chem. A*, vol. 9, no. 38, pp. 22015–22024, 2021, https://doi.org/10.1039/d1ta03894j.
54. Y. Zhao, X. Q. Liu, S. Y. Wu, and X. M. Chen, "Electrocaloric effect and pyroelectric energy harvesting in diffuse ferroelectric Ba(Ti1-xCex)O3 ceramics," *J. Electroceramics*, vol. 43, no. 1–4, pp. 106–116, Dec. 2019, https://doi.org/10.1007/s10832-019-00183-6.

Arrived: 22. 05. 2024
Accepted: 12. 09. 2024